

Investigation of seasonal changes in lipid synthesis and metabolism-related genes in the oviduct of Chinese brown frog (*Rana dybowskii*)

Yankun Wang,* Yuning Liu,* Yawei Wang, Ao Zhang, Wenqian Xie, Haolin Zhang, Qiang Weng, Meiyu Xu
College of Biological Sciences and Technology, Beijing Forestry University, Beijing, China

*These authors contributed equally to this work.

ABSTRACT

A peculiar physiological characteristic of the Chinese brown frog (*Rana dybowskii*) is that its oviduct dilates during pre-brumation rather than during the breeding season. This research aimed to examine the expression of genes connected with lipid synthesis and metabolism in the oviduct of *R. dybowskii* during both the breeding season and pre-brumation. We observed significant changes in the weight and size of the oviduct between the breeding season and pre-brumation. Furthermore, compared to the breeding season, pre-brumation exhibited significantly lower triglyceride content and a marked increase in free fatty acid content. Immunohistochemical results revealed the spatial distribution of triglyceride synthase (Dgat1), triglyceride hydrolase (Lpl and Hsl), fatty acid synthase (Fasn), and fatty acid oxidases (Cpt1a, Acadl, and Hadh) in oviductal glandular cells and epithelial cells during both the breeding season and pre-brumation. While the mRNA levels of triglycerides and free fatty acid synthesis genes (*dgat1* and *fasn*) did not show a significant difference between the breeding season and pre-brumation, the mRNA levels of genes involved in triglycerides and free fatty acid metabolism (*lpl*, *cpt1a*, *acatl*, *acox* and *hadh*) were considerably higher during pre-brumation. Furthermore, the *R. dybowskii* oviduct's transcriptomic and metabolomic data confirmed differential expression of genes and metabolites enriched in lipid metabolism signaling pathways during both the breeding season and pre-brumation. Overall, these results suggest that alterations in lipid synthesis and metabolism during pre-brumation may potentially influence the expanding size of the oviduct, contributing to the successful overwintering of *R. dybowskii*.

Key words: brumation; lipid metabolism; lipid synthesis; oviduct; *Rana dybowskii*.

Correspondence: Meiyu Xu, Ph.D., College of Biological Sciences and Biotechnology, Beijing Forestry University, Beijing 100083, China. E-mail: xumeiyu@bjfu.edu.cn

Contributions: Yankun Wang, data curation, methodology, writing original draft; Yuning Liu, data curation, writing original draft, editing; Yawei Wang, investigation, data curation; Ao Zhang, investigation, methodology, data curation; Wenqian Xie, methodology, data curation; Haolin Zhang, resources, conceptualization, funding acquisition; Qiang Weng, conceptualization, resources, funding acquisition; Meiyu Xu, writing original draft, conceptualization, data curation.

Conflict of interest: the authors declare that they have no competing interests.

Ethics approval: all animal testing procedures were approved by the Animal Protection and Utilization Policy of the Beijing Forestry University Ethics Committee (EAWC_BJFU_202008).

Funding: this study is supported by a Grant-in-Aid from Beijing Natural Science Foundation (7232240; 6222042) and National Natural Science Foundation of China (31872320).

Introduction

Many metamorphic vertebrates, including amphibians, enter a quiescent state known as dormancy, hibernation or brumation (*i.e.*, the dormant state for amphibians and reptiles).^{1,2} Hibernators exhibit remarkable physiological changes, such as reduced body core temperature, slow breathing and heart rate, and reduced systemic metabolism, to adapt to cold temperatures and food scarcity during winter.^{3,4} These adaptations allow animals to expend relatively less heat during winter.⁴ Lipid reserves are the energy budget of an organism and are usually located in the abdominal fat or the tail of amphibians.⁵ Lipids are utilized for the development of gonadal cells and serve as an energy storage during brumation or torpor in ectotherms.⁵ Adult salamanders use lipids in their bodies during prolonged starvation, and more giant amphibians are generally better able to resist starvation.⁵

It is widely accepted that the importance of lipid storage and lipolysis in hibernation/brumation.⁶ For instance, gecko (*Phyllodactylus marmoratus*) and the common lizard (*Lacerta vivipara*) rely on lipid storage during brumation.⁷ Australian frogs accumulate about 24% of their total body weight as lipids within the pads of their feet in preparation for long-term dormancy.⁸ In the mountain yellow-legged frog (*Rana muscosa*), frogs with higher relative mass have higher recapture rates between years, indicating the survival advantage of individuals with more lipid.⁵ Therefore, sufficient lipid storage is crucial for the survival of hibernating or brumating animals during the winter.

During periods of fasting, hibernating/brumating animals obtain most of their energy from lipid reserves.⁹ Adipose tissue expansion occurs through adipocyte formation, a process collectively known as adipogenesis, which involves the accumulation of triglycerides (TGs) within lipid droplets.¹⁰ TGs are stored in lipid droplets of the cytoplasm and are made up of glycerol and fatty acids.^{11–13} The accumulation of lipids in both vertebrates and invertebrates is greatly influenced by fatty acid synthase (Fasn).¹⁴ It is responsible for *de novo* lipogenesis, converting acetyl coenzyme A (acetyl-CoA) to palmitate, leading to the production and storage of TGs.¹⁴ Diacylglycerol acyltransferases (Dgat), including Dgat1 and Dgat2, are responsible for catalyzing the synthesis of TGs using acetyl-CoA.¹⁵ Dgat1 has broader substrate specificity (for acyl acceptors) than Dgat2.¹⁵

When the mobilization of endogenous energy stores is required, such as during fasting and exercise, TGs are hydrolyzed through lipolytic processes and released into the circulation as free fatty acids (FFA).¹³ TG can be hydrolyzed to glycerol and FFA by enzymes such as hormone-sensitive lipase (Hsl) and lipoprotein lipase (Lpl).¹⁶ Hsl is an enzyme that acts on various substrates and is considered the rate-limiting agent of the lipolysis process.¹⁷ Lpl is a central enzyme in lipid metabolism, capable of hydrolyzing TG from celiac particles and very low-density lipoproteins.¹⁸ Oxidation of fatty acids from TGs catabolism promotes heat production to maintain core body temperature.¹⁹ Fatty acids are catabolized to produce energy through processes such as beta-oxidation in cellular mitochondria.²⁰ This catabolic process breaks down fatty acid molecules into smaller units, such as acetyl-CoA, which then enter the citric acid cycle to produce ATP.²⁰ In fasting, the process of mitochondrial fatty acid oxidation is activated, whereby the oxidation rate of long-chain fatty acids is primarily regulated by the enzyme carnitine palmitoyltransferase 1 (Cpt1), which acts as a limiting factor.²¹ The Cpt1 protein family contains three isoforms: Cpt1a, Cpt1b and Cpt1c, with Cpt1a being commonly expressed in various tissues throughout the body and primarily responsible for energy metabolism.²² Long-chain acyl-coenzyme A dehydrogenase (Acadl) is a critical enzyme in the initial step of fatty acid β -oxidation.²³ Peroxisomal β -oxidation involves the pro-

cessing of various fatty acid substrates, acted upon by two or three distinct acyl-CoA oxidase (Acox) enzymes exhibiting varying specificities.²⁴ Eukaryotes also employ peroxisomal β -oxidation, catalyzed by acyl-CoA oxidase (Acox), instead of Acad proteins.²⁵ Acox proteins exhibit a notable sequence similarity with Acad proteins, and they also catalyze the conversion of acyl-CoA to enoyl-CoA.²⁵ Studies suggest that Acoxs play a significant role in addressing oxidative stress caused by environmental xenobiotics, in addition to their essential functions in fatty acid oxidation and maintaining redox balance.²⁶ The *hadh* gene encodes short-chain L-3-hydroxy acyl-CoA dehydrogenase, a key enzyme in fatty acid β -oxidation responsible for catalyzing the third stage of mitochondrial fatty acid oxidation.²⁷ Many hibernating animals utilize increased fatty acid catabolism as a survival strategy.²⁸

The Chinese brown frog (*Rana dybowskii*) is a species belonging to the Chordata, Amphibia, Anura, Ranidae, and *Rana* classifications. As a seasonal breeding brumating amphibian influenced by factors such as latitude and altitude, *R. dybowskii* typically brumates from October to February and breeds from February to June.^{29,30} *R. dybowskii* seeks quiet environments with low water currents, such as river bays, spring pits, and areas with layers of dead branches and leaves during brumation. A distinct physiology of *R. dybowskii* is that its oviducts dilate before brumation rather than during the breeding season.^{31,32} The dried product of the dilated oviduct, known as *Oviductus Ranae*, is widely used in traditional Chinese medicine due to its nourishing properties for Yin, lung moisture, and kidney essence replenishment.^{33,34} *Oviductus Ranae* contains a variety of nutrients, with proteins and lipids being the most significant components, with lipid content of up to 50%.³⁴

Previous studies have shown that genes related to glycolysis and glycogenesis are upregulated.² In contrast, genes related to gluconeogenesis decrease during pre-brumation in *R. dybowskii*, suggesting that glycogen accumulation plays a role in oviductal proliferation and differentiation.² However, in *R. dybowskii*, further in-depth research is needed to investigate the mechanisms of lipids synthesis and metabolism in the oviductal expansion before brumation. Hence, the main aim of our current investigation is to examine the genes and protein expression patterns associated with lipid synthesis and metabolism in the oviduct of *R. dybowskii* during the breeding season and pre-brumation. The objective is to explore the relationship between lipid synthesis, metabolism, and oviductal expansion during pre-brumation, thereby deepening the comprehension of the control of oviductal hypertrophic.

Materials and Methods

Animals

A total of 54 female *R. dybowskii* specimens were acquired from a *R. dybowskii* farm located in Jilin City, Jilin Province, China. The animals were obtained during two distinct periods: the breeding season in April 2019 (n=27) and pre-brumation in September 2018 (n=27). The geographical coordinates of the farm are around the longitudes of 125°40'E–127°56'E and the latitudes of 42°31'N–44°40'N. The animals used in the laboratory were handled in compliance with the requirements of the Beijing Forestry University Ethics Committee regarding the treatment and utilization of animals. Anesthesia with ether was administered to the female *R. dybowskii*, followed by a dissection of their oviductal tissues on both sides of the abdomen. The tissues were then weighed and recorded, and the diameter of the oviduct was measured by assessing its circumference. One side of the oviduct was sectioned into 1–2 cm segments, then immersed in a previously prepared paraformaldehyde solution (using Tait's solution), and

finally preserved for long-term storage in a 70% ethanol solution. The other part of the oviduct was preserved in a freezer at a temperature of -80°C for long-term storage and used for Oil red O staining, transcriptome and metabolome sequencing, as well as RNA extraction.

Determination of triglycerides and free fatty acids content

TGs were hydrolyzed to produce glycerol and fatty acids after saponification. Subsequently, glycerol underwent oxidation using periodate as a reagent, resulting in the formation of formaldehyde. Under the influence of chloride ions, the reaction between formaldehyde and acetylacetone led to the synthesis of a yellow compound with a distinct at 420 nm. The TG levels in the oviductal tissue were quantified using the Solarbio Life Science (Beijing, China) Triglyceride Content Assay Kit (BC0625) according to the manufacturer's instructions. The absorbance measurement for each treatment was conducted using a reader for microplates (Multiskan FC Enzyme Labeler; Bio-Rad, Hercules, CA, USA).

The concentrations of the oviductal tissue FFA were determined using the Free fatty acid Assay Kit (AK231) according to the manufacturer's instructions (Bioss, Beijing, China). In brief, approximately 0.1 g of oviduct tissue was weighed, 1.0 mL of reagent A was added, and the tissue was homogenized on ice. After centrifugation (8,000 rpm, 4°C , 10 min), the supernatant was collected, and the samples were added and mixed with trichloromethane; then reagent B and reagent C were added. Centrifugation (3,000 rpm, 4°C , 10 min) was performed after sufficient shaking and the upper solution (50 μL) was taken. The FFA content was measured by recording the absorbance at 550 nm (Multiskan FC Enzyme Labeler; Bio-Rad) after introducing reagent D into the supernatant and incubating for 15 min at room temperature.

Histological observations

For hematoxylin-eosin (H&E) staining, the samples of the oviduct were embedded in paraffin after dehydration in an ethanol series. The paraffin wax was sliced to a thickness of 5 μm using a rotating microtome (ES-A01-YD-315; Yidi, Jinhua China). The serial sections were affixed onto slides that had been treated with poly L-lysine (Sigma, St. Louis, MO, USA), and afterward subjected to a drying process. They were deparaffinized three times in xylene for 5 min each and subsequently rehydrated in graded ethanol (100%, 95%, 90%, 80%, and 70%) for 5 min each. Hematoxylin staining was performed for 20 s, followed by rinsing with running water for 25 min. Eosin staining was then carried out for 4 min, and the sections were dehydrated with increasing concentrations of the graded ethanol for 3 min each. Finally, the H&E-stained sections were sealed with neutral resin for histological observation. Frozen oviductal tissue was cut to a thickness of 6 μm using a cryostat (CM1100, Leica, Wetzlar, Germany). Frozen sections were fixed by adding paraformaldehyde solution dropwise for 10 min. Afterward, they were washed three times in a 60% isopropanol solution for 4 min each time. The sections were then spotted with Oil Red O staining treatment for 20 min. Following that, they were washed three times in a 60% isopropanol solution for 4 min each time. Hematoxylin was applied for 20 s, after which they were treated in tap water for 25 min. Finally, the sections were sealed with neutral resins for observation. Oil Red O-stained slides were examined using an Olympus microscope (BX51, Olympus, Tokyo, Japan) with a 20x objective. Three slides were prepared as replicates for Oil Red O staining for each of the two periods of the breeding season and pre-brumation. Each slide contained three frozen sections. The intensity of the red color was observed, and images were captured using a BX51 Olympus microscope.

Immunohistochemistry

Immunohistochemistry (IHC) experiments were performed using the KeyGEN One-Step IHC Assay (DAB, compatible for Rabbit and Mouse). According to the manufacturer's instructions, 5 μm paraffin sections were deparaffinized with xylene, rehydrated, and subjected to antigen retrieval using 10 nM citrate buffer; microwave heating was performed at a high temperature for 5 min, followed by a 5 min interval at room temperature. Subsequently, heating at a medium-high temperature for 5 min was carried out, again followed by a 5 min interval at room temperature. Finally, heating at a low temperature for 5 min was performed. After the citrate solution returned to room temperature, the slides were washed with PBS. The sections were then immersed in a 3% H_2O_2 -methanol solution for 10 min to eliminate the action of endogenous catalase, and subsequently rinsed three times with 0.05 M PBS (pH 7.4) for 5 min each. Reagent A (10% goat serum blocking solution) was applied to the tissue sections and incubated for 30 min. Primary antibodies, including rabbit anti-DGAT1 antibody (bs-2332R; 1:100 dilution; Bioss), rabbit anti-LPL antibody (ab172953; 1:100 dilution; Abcam, Cambridge, UK), rabbit anti-HSL/LIPE antibody (bs-0455R, 1:100 dilution; Bioss), rabbit anti-FASN antibody (bs-1498R, Bioss; 1:100 dilution), rabbit anti-CPT1A antibody (bs-2047R, 1:100 dilution; Bioss), rabbit Anti-ACADL antibody (bs-5015R, 1:100 dilution; Bioss), and rabbit anti-HADH antibody (19828-1-AP, 1:100 dilution; Proteintech, Rosemont, IL, USA) were added, and negative controls were treated with PBS. The sections were incubated overnight at 4°C with the primary antibodies. The primary antibody solution was removed, and each section was incubated for 30 min with the addition of reagent B (enhancer). The sections were then washed three times with PBS for 2 min each. Subsequently, reagent C (HRP polymer) was applied to each section and incubated for 30 min. The sections were again washed 3 times with PBS for 2 min each. Staining was performed using DAB chromogenic solution, and distilled water was used as the termination solution. The nuclei were counterstained with hematoxylin. Finally, the slices were dehydrated and sealed with neutral gum. Immunostained slides were examined with a BX51 microscope (Olympus), using a 20x objective. For each antibody case, three slide replicates were prepared, each containing four paraffin sections of oviduct tissue, during both the breeding season and pre-brumation. The location of the positive signal in the oviduct was observed, and the intensity of DAB staining-positive signals was quantified using ImageJ (version 1.53k, National Institutes of Health, Bethesda, MD, USA). The common categories describing IHC expression during the breeding season and pre-brumation were classified as follows: negative (-), weak (+), moderate (++), and strong (+++), depending on the average optical density of DAB staining.

Isolation of RNA

The isolation of total RNA from oviductal tissue samples was carried out using a Trizol[®] kit (Invitrogen, Carlsbad, CA, USA), based on the manufacturer's instructions. Around 0.1 g of oviductal tissue were promptly homogenized in 1 mL of Trizol reagent through a high-frequency homogenizer. Then, adding 0.2 mL of chloroform, the mixture was stirred vigorously for about 30 s, and left at room temperature for 5 min. Next, the supernatant was transferred to a new tube and isopropyl alcohol (Beijing Hongda Kelai Technology Co., Ltd.) equivalent to 80% of the supernatant was added. To collect RNA, the samples were spun at 12,000 g for 15 min at 4°C . The RNA pellet was dissolved in 40 μL of diethyl carbonate-treated water (Beijing Hongda Collet Technology Co., Ltd., Beijing, China) after cleansing it three times with 75% cold ethanol, letting the remaining ethanol dry in the air.

Construction and sequencing of RNA library

Following the protocol offered by the manufacturer of the Trizol[®] kit, total RNA was isolated from *R. dybowskii* oviduct parts. The extracted total RNA sample was then used to isolate poly(A) mRNA using magnetic beads (Invitrogen) attached to a poly (T) oligo-element. The Bioanalyzer 2100 and RNA 6000 Nano LabChip kit (Agilent, Santa Clara, CA, USA) quantified and purified total RNA with a RIN score of over 7.0, indicating good RNA quality. Following the steps in the mRNA-seq sample preparation kit (Illumina, San Diego, CA, USA), the pure mRNA was broken up randomly and reverse-transcribed to make cDNA libraries.

qRT-PCR

The cDNA strands were synthesized using a kit from GenStar (Beijing, China) called Star-Script II First-strand cDNA Synthesis Kit. The primers used for qRT-PCR analyses were designed *via* the NCBI Primer-BLAST program (Table 1). For the qRT-PCR process, a 10 μ L volume was prepared, adding 3 μ L of cDNA, 5 μ L of 2 \times SG Green qPCR Mix, 0.1 μ L of both reverse and forward primer at a concentration of 10 μ M, and 1.8 μ L of nuclease-free water. The mixture was thoroughly mixed and added to the 96-well PCR plate following the designed protocol. The qRT-PCR reactions were performed using the ABI PRISM 7500 fast real-time PCR system (Applied Biosystems, Foster City, CA, USA) with an initial denaturation at 95°C for 10 min, followed by 40 cycles of denaturing at 95°C for 30 s, annealing at 60°C for 30 s, and extension at 70°C for 30 s. The expression levels of target genes levels were compared to the house-keeping gene *beta-actin* and determined with the 2^{- $\Delta\Delta$ C_t} method.

Transcriptome data analysis

Initially, the collected information in FASTQ format was processed using an internal Perl script (Biomarker Biotechnology, Beijing, China). In this stage, the raw reads underwent preprocessing using a cut adaptor (v1.9.1) to exclude reads containing adapters, ploy-N sequences longer than 10%, and low-quality reads with a mass fraction less Q30 (85%). Quality metrics such as Q30 scores, GC percentage, and sequence repeat counts were determined for the clean data. Clean reads were defined as high-

quality reads that met the quality standards and were encoded in FASTQ format.³⁵ The transcriptomic results were treated with Kyoto Encyclopedia of Genes and Genomes (KEGG) enrichment. In the end, the visualization and plotting of the results using Bioinformatics (<https://www.bioinformatics.com.cn/>) and Chiplot (<https://www.chiplot.online/>).

Metabolite extraction and metabolome analysis

Oviductal samples were prepared with reference to those mentioned in previous publications, with some modifications.^{36,37} 25 mg of oviduct tissue was weighed, and six biological replicates were used for each of the breeding season and pre-brumation. 500 μ L extract solution (acetonitrile:methanol:water, 2:2:1) containing isotopically-labelled internal standard (L-2-Chlorophenylalanine) mixture was added. After vortexing for 30 s, tissue was homogenized for 4 min at 35 Hz and sonicated for 5 min in the ice water bath. The cycles of homogenization and sonication were repeated 4 times. The samples were then incubated for 1 h at -40°C, and then centrifuged (12,000 rpm, 4°C) for 15 min. 400 μ L of supernatant was taken and dried at 37°C in a vacuum concentrator. Desiccated samples were added to 100 μ L of 50% acetonitrile and mixed well. After centrifugation (13,000 rpm at 4°C) for 15 min, the supernatant was used for ultra performance liquid chromatography tandem mass spectrometry (UPLC/MS) analysis. From each sample, a mixture of 10 μ L was taken as a quality control sample.

UPLC separations were performed using a 1290 Infinity series UPLC system (Agilent) with a UPLC BEH amide column (2.1 \times 100 mm, 1.7 μ m, Waters Corporation, Milford, CT, USA). Mobile phase A was 25 mmol/L ammonium acetate and 25 mmol/L ammonium hydroxide aqueous solution (pH 9.75) and mobile phase B was acetonitrile. Analyses were performed using the following elution gradients: 95% mobile phase B, 0 to 0.5 min; 95% to 65% mobile phase B, 0.5 to 7.0 min; 65% to 40% mobile phase B, 7.0 to 8.0 min; 40% mobile phase B, 8.0 to 9.0 min; 40% to 95% mobile phase B, 9.0 to 9.1 min; and 95% mobile phase B, 9.1 to 12.0 min. The column temperature was set at 25°C. The injection volume was 2 μ L for each of the positive and negative ion modes. ESI source conditions were set as follows: gas 1 as 60 psi, gas 2 as 60 psi, curtain gas as 35 psi, source temperature as 600°C, declustering potential as 60 V, Ion spray voltage floating (ISVF) as 5000 V or -4000 V in positive or negative modes, respectively. The

Table 1. Primers sequence used for mRNA q-PCR.

Gene names	Primer sequence	Product length (bp)
<i>dgat1</i>	F:5'-GGCAACCTGACACACAGAGA-3' R:5'-ATGAGATGATTGGGGACCGC-3'	266
<i>fasn</i>	F:5'-GGCGGGGATAAAAAGATGGAGT-3' R:5'-CGAGAGGTGAGCACCAAGTT-3'	303
<i>hsl</i>	F:5'-CCAAGTCCCACGAACCCTAC-3' R:5'-CCAGCACTGTCACTGCTAA-3'	202
<i>hadh</i>	F:5'-CAGAGCACTTGGAAAGACGC-3' R:5'-CGCTCATAAAGCGGACTGA-3'	105
<i>acadd</i>	F:5'-ACACTTAAAGGCGCGTCACT-3' R:5'-GGTGGACCAATGAGATTATGA-3'	153
<i>acox</i>	F:5'-ACAAAAGCCATCCGCACAAC-3' R:5'-ACCATCACTCTGGCATTGG-3'	233
<i>beta-actin</i>	F:5'-AACCTCTTAGAAACCGGCA-3' R:5'-AAGCGTAAAGTGCCAGGTTG-3'	103
<i>cpt1a</i>	F:5'-TCAGAGCTCCCTGGCTGTTG-3' R:5'-TTCCCTCTCGAAAAGTCGG-3'	212
<i>lpl</i>	F:5'-CCAGACCGTAGCATAGGCAT-3' R:5'-CTGTAAAGCCCCGTAGACCT-3'	136

TripleTOF 6600 mass spectrometry (AB Sciex, Framingham, MA, USA) was used for its ability to acquire MS/MS spectra on an information-dependent basis (IDA) during an LC/MS experiment. Search for metabolite pathways using KEGG (<http://www.kegg.jp>) and MetaboAnalyst (<http://www.metaboanalyst.ca/>). Screening for differential metabolites in combination with multiplicative changes and VIP values from the OPLS-DA model. Finally, data visualisation was done using Chiplot (<https://www.chiplot.online/>).

Statistical analysis

A statistical evaluation of the data was conducted using GraphPad Prism 8 analytical software. Student's *t*-test was selected to assess significant differences. A *p*-value >0.05 was considered not significant, while *p*<0.05 was considered significant, *p*<0.01 was regarded as very significant, and *p*<0.001 was considered extremely significant.

Results

Morphological and histological changes in the oviduct of *Rana dybowskii*

During the breeding season and pre-brumation, the oviduct of *R. dybowskii* showed morphological and histological alterations (Figure 1). The oviduct underwent specific enlargement in pre-brumation, displaying a notable increase in size in comparison to the breeding season (Figure 1a). Additionally, there was a notable increase in both the weight and width of the oviduct in pre-brumation, in comparison to the values recorded during the breeding season (Figure 1 b-d). The oviduct comprised three parts: glandular cells (GC), epithelial cells (EC) and the tubal lumen (TL), arranged from outer to inner layers (Figure 1 e,f). During the breeding season, the cell nucleus was visible, and the GC were small in size (Figure 1e). Conversely, in pre-brumation, the size of GC increased, and the nucleus became difficult to observe (Figure 1f).

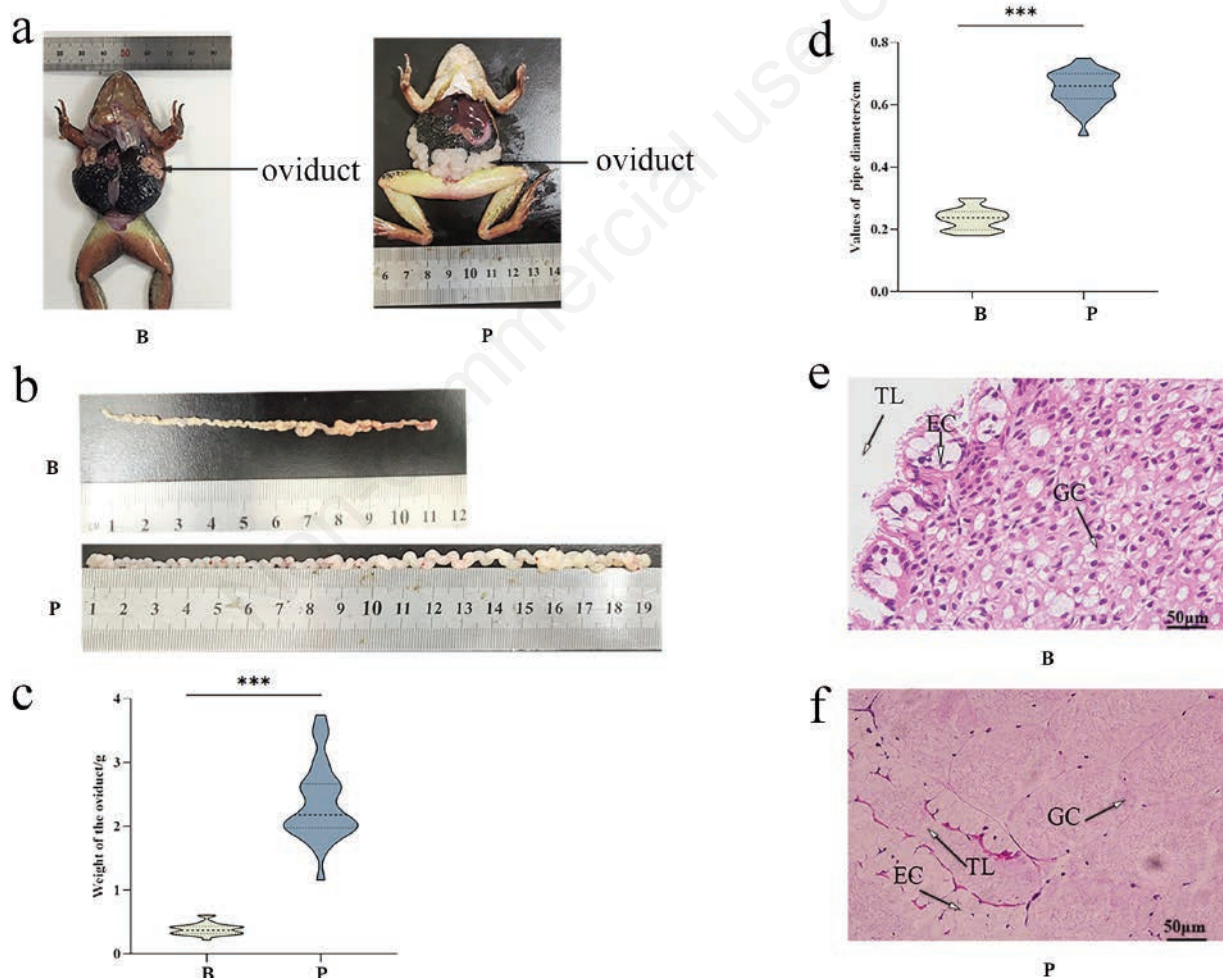


Figure 1. Morphological and histological observations of the oviduct in *R. dybowskii*. **a**) The anatomical positioning of the oviduct throughout the two periods in *R. dybowskii*. **b**) A comparative analysis of the morphological alterations occurring in the oviduct throughout the two periods. **c**) Weight of the oviduct in two periods. **d**) Pipe diameter of the oviduct in two periods. H&E staining during the breeding season **(e)** and pre-brumation **(f)**. Mean \pm SEM were plotted. Three biological repeats were used for each period; GC, glandular cell; EC, epithelial cell; TL, tubal lumen; B, breeding season; P, pre-brumation; scale bars: 50 μ m; ****p*<0.001.

Localization of triglycerides, and content of triglycerides and free fatty acids

The localization and content of TG in *R. dybowskii*'s oviduct were examined during the breeding season and pre-brumation (Figure 2). Oil red O staining was utilized to stain lipids. During the breeding season, the GC in the oviduct exhibited more intense staining, indicating a higher lipid content (Figure 2a). In contrast, during pre-brumation, the ciliated portion of the EC showed faint staining (Figure 2b). Subsequently, we quantified TG content using a commercial triglyceride content assay kit and found that during pre-brumation, the TG content in the oviduct of *R. dybowskii* was significantly lower than during the breeding season (Figure 2c). To explore whether the observed decrease in TG during winter resulted from hydrolysis into FFA, we further measured the FFA content. In contrast to TG content, FFA levels exhibited a notable increase before brumation compared to the breeding season (Figure 2d).

Immunolocalization of Dgat1, Lpl, Hsl, Fasn, Cpt1a, Acadl and Hadh

Our results revealed lower TG and higher FFA levels during pre-brumation compared to the breeding season. To further investigate the expression of enzymes involved in TG and FFA synthesis and hydrolysis, we examined the expression pattern of TG synthase Dgat1, TG hydrolase Lpl and Hsl, fatty acid synthase Fasn, and fatty acid oxidases Cpt1a, Acadl and Hadh in the oviduct of *R. dybowskii* using IHC (Figure 3). Interestingly, these enzymes

exhibited different spatial expression patterns in the oviduct between the breeding season and pre-brumation. Specifically, during the breeding season, the TG and FFA synthases, Dgat1 and Fasn mainly displayed positive signals in GC, while during pre-brumation, these signals were primarily found in EC (Figure 3 a-b,g-h). Furthermore, enzymes responsible for TG and FFA hydrolysis, namely Lpl, Hsl, Cpt1a, Acadl, and Hadh, exhibited a similar expression pattern: during the breeding season, the immunopositivity was mainly observed in GC, whereas during pre-brumation, it was present in both GC and EC (Figure 3 c-f, i-n). No IHC signal was detected in the negative control (Figure 3 o,p). Table 2 reports the relative expression of each antibody in GC and EC during the breeding season and pre-brumation.

mRNA expressions of *dgat1*, *lpl*, *hsl*, *fasn*, *cpt1a*, *hadh*, *acadl* and *acox*

We further examined the mRNA level of those key enzymes involved in TG synthesis and hydrolysis, as well as FFA synthesis and oxidation, during both the breeding season and pre-brumation (Figure 4). Our analysis revealed that there were no discernible changes in the mRNA levels of *dgat1*, *fasn*, and *hsl* transcripts, indicating a consistent TG and FFA synthesis profile between the two observed periods. However, the mRNA expression of *lpl*, *cpt1a*, *acadl*, *acox* and *hadh* was significantly upregulated during pre-brumation, which is consistent with the decrease in TG levels and the increase in FFAs during the pre-brumation period, as shown above.

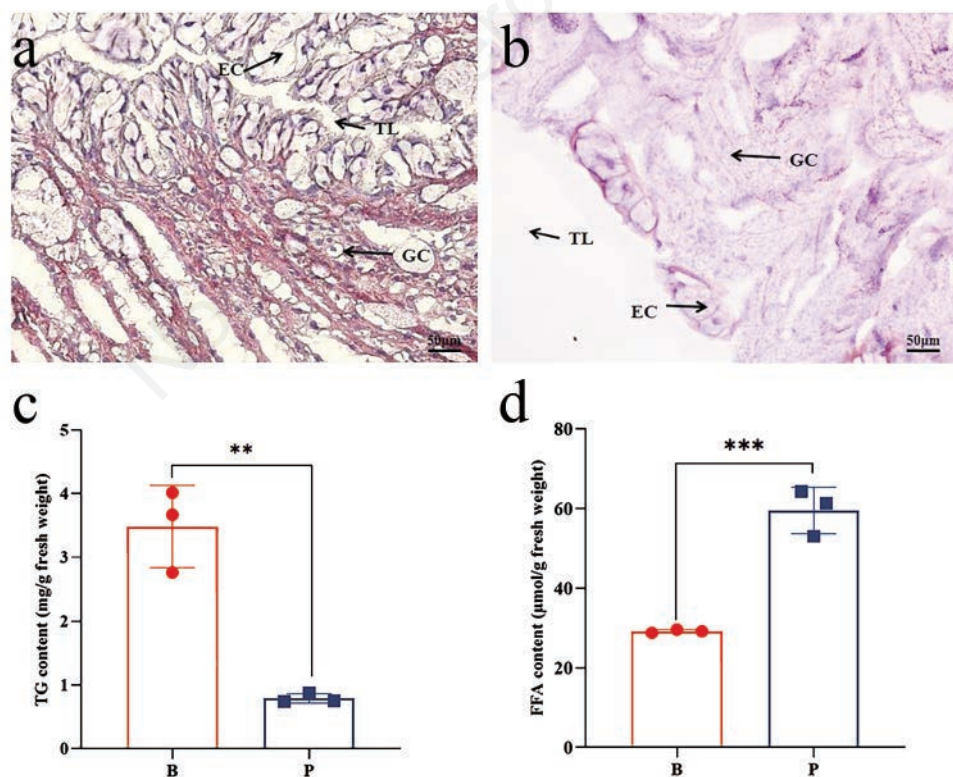


Figure 2. Localization of TG and content of TG and FFA. TG localization of the oviduct in *R. dybowskii* during the breeding season (a) and pre-brumation (b). Quantification of TG (c) and FFA (d) content of the oviduct. The scale lines were 50 μm. Mean ± SEM were plotted. GC, glandular cell; EC, epithelial cell; TL, tubal lumen; B, breeding season; P, pre-brumation. Three biological repeats were used for each period; **p<0.01.

Analysis of the KEGG map and heat map of transcriptome data

Transcriptome analysis revealed the involvement of ten pathways related to lipid metabolism, including the peroxisome proliferator-activated receptor (PPAR) signaling pathway, linoleic acid metabolic process, glycerophospholipid metabolic process, glyce-

rolipid metabolic process, fatty acid elongation, fatty acid degradation, unsaturated fatty acid biosynthesis, arachidonic acid metabolic process, α -linolenic acid metabolic process, and adipocytokine signaling pathway. Among these pathways, fatty acid degradation exhibited the highest number of differentially expressed genes (DEGs) (Figure 5a).

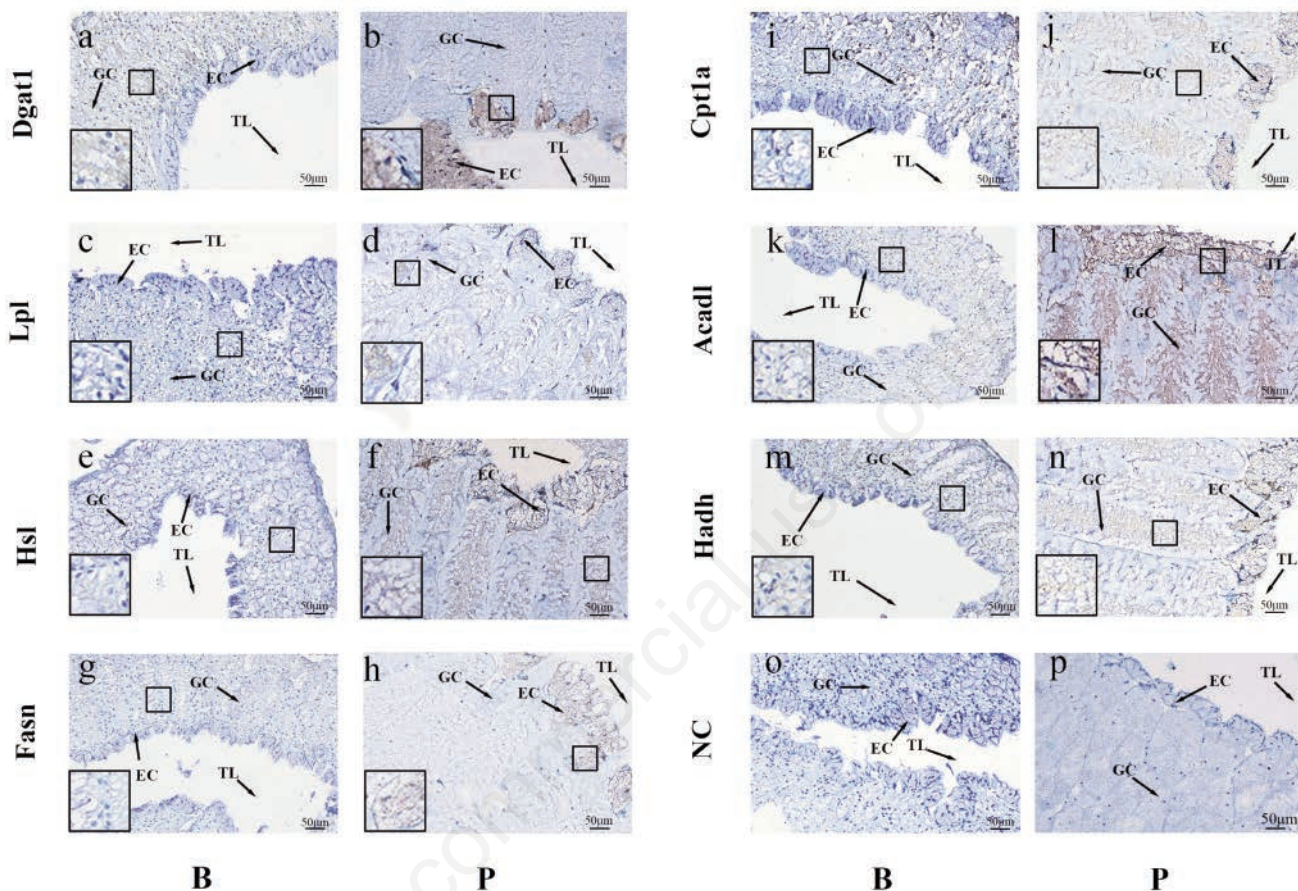


Figure 3. Immunolocalization of TG and FFA synthases and hydrolases in the oviduct of *R. dybowskii*. The immunolocalization of Dgat1, Lpl, Hsl, Fasn, Cpt1a, Acadl and Hadh in the oviduct of *R. dybowskii*. The first (a,c,e,g) and third (i,k,m,o) columns showed positive signaling in breeding season. The second (b,d,f,h) and fourth (j,l,n,p) columns showed positive staining during pre-brumation. Immunolocalization of Dgat1 (a,b), Lpl (c,d), Hsl (e,f), Fasn (g,h), Cpt1a (i,j), Acadl (k,l), and Hadh (m,n) in the oviduct of *R. dybowskii*. No immunostaining was observed in the negative control (o,p) sections. EC, epithelial cell; TL, tubal lumen; NC, negative control. B, breeding season; P, pre-brumation; scale bars: 50 μ m.

Table 2. Relative abundance of Dgat1, Lpl, Hsl, Fasn, Cpt1a, Acadl and Hadh in the oviduct of *Rana dybowskii* during the breeding season and pre-brumation

Antibodies	B		P	
	EC	GC	EC	GC
Dgat1	+	++	+++	+
Lpl	+	++	++	++
Hsl	+	+	++	++
Fasn	+	+	++	+
Cpt1a	+	++	++	++
Acadl	+	++	+++	+++
Hadh	+	++	+++	+++
NC	-	-	-	-

B, breeding season; P, pre-brumation; GC, glandular cell; EC, epithelial cell; TL, tubal lumen; -, negative; +, weak; ++, moderate; +++, strong.

The heat map (Figure 5b) showed that DEGs associate with the PPAR signaling pathway (*dbi*, *acac1*, *acox1*), fatty acid degradation (*hadh*, *acac1*, *acox1*, *aldh9a1*), glycerophospholipid metabolic process (*mboat7*, *adprm*, *lpcat4*, *pcyt1a*, *gpd1*), linoleic acid metabolic process (*cyp2c8*, *cyp3a4*, *cyp3a5*), arachidonic acid metabolic process (*cyp2c8*, *itc4s*), and α -linolenic acid metabolic process (*acox1*) were significantly upregulated during pre-brumation. In contrast, the adipocytokine signaling pathway (*nfkbia*, *pck1*, *irs1*), and insulin signaling pathways (*soc2*, *irs1*, *ptprf*, *irs2*, *pck1*) were significantly upregulated during the breeding season.

Analysis of the Lollipop chart map and column chart map of metabolomics data

The results of this metabolome were based on the analysis of positive ion patterns. A Lollipop chart map representing the differential metabolites of the lipid metabolism pathway was generated using ChiPlot (Figure 6a). During the breeding season and pre-brumation, there were a total of 25 metabolites that showed differential expression. In pre-brumation, 18 metabolites showed upregulation, while 7 metabolites showed downregulation.

The results of KEGG analysis for lipid metabolism-related metabolome differences were visualized using a column chart (Figure 6b). The chart showed the eight most significant pathways of enrichment, namely glycerolipid metabolism, linoleic acid metabolism, glycerophospholipid metabolism, α -linolenic acid metabolism, biosynthesis of unsaturated fatty acids, fatty acid degradation, arachidonic acid metabolism, and fatty acid biosynthesis.

Discussion

This study presents novel findings regarding the expression patterns of genes responsible for lipid synthesis and metabolism during pre-brumation in the oviduct of *R. dybowskii*.

Our results showed lower TG levels and higher levels of FFA, a product of TG hydrolysis, during pre-brumation compared to the breeding season. IHC results confirmed the expression pattern of

TG and FFA synthase and hydrolase enzymes, including *Dgat1*, *Lpl*, *Hsl*, *Fasn*, *Cpt1a*, *Acadl*, and *Hadh*, in the oviduct during both the breeding season and pre-brumation. Furthermore, the mRNA levels of *lpl*, *cpt1a*, *acac1*, *acox* and *hadh*, which are associated with TG hydrolysis and FFA oxidation, were significantly elevated in pre-brumation compared to the breeding season. Additionally, the transcriptomics and metabolomics results of the oviduct indicated that DEGs and differential metabolites are involved in lipid metabolism-related pathways, including fatty acid degradation, linoleic acid metabolism, and α -linolenic acid metabolism. The graphical summary of lipid metabolism in the oviduct is shown in Figure 7. These findings suggest that the increased heat generation resulting from the oxidation of fatty acids in the oviduct before brumation may play a significant role in the effective overwintering of *R. dybowskii*.

A peculiar physiological phenomenon observed in *R. dybowskii* is the specific enlargement of its oviduct during pre-brumation rather than the breeding season.² The present findings provide additional experimental evidence that the structure and morphology of the oviduct differ significantly between the pre-brumation and the breeding season. In contrast to the breeding season, pre-brumation is characterized by an expansion of oviductal tissue, a significant increase in GC size, as well as an increase in oviduct weight and volume. Therefore, the current results further support the hypothesis that the oviduct experiences an increase in weight and volume before brumation. These findings are consistent with our previous studies.^{2,31,33,34} However, in studies on the Argentine shortfin squid, it has been found that the reproductive organs (ovary and oviduct) account for an increasing proportion of energy during sexual maturation, building up energy for reproduction.³⁸ Different from non-breeding, the weight and length of the oviduct in guinea hens (*Numida meleagris*) displayed increased values during the breeding season.³⁹ In passerine birds, observations conducted throughout both the non-breeding and breeding seasons have shown that the wet mass of the oviduct experiences a substantial rise, reaching up to a 220-fold augmentation during the breeding season.⁴⁰ Based on these pieces of evidence and the findings of the current study, it is believed that the oviductal expansion in *R.*

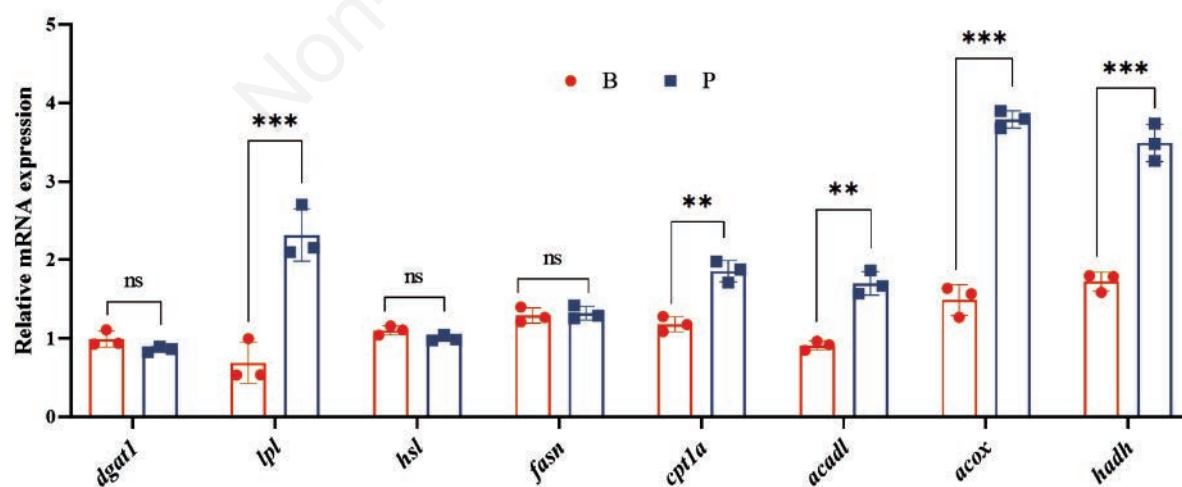


Figure 4. Gene expression levels for lipid synthesis and metabolism were evaluated. The investigation focused on analyzing the mRNA transcript levels of the genes *dgat1* and *fasn*, which are known to be associated with lipid synthesis and fatty acid synthesis. The levels of transcription of *lpl*, *hsl*, *cpt1a*, *acac1*, *acox* and *hadh* mRNA are associated with the process of TG hydrolysis and fatty acid oxidation. Mean \pm SEM were shown. Three biological repeats were used for each period. B, breeding season; P, pre-brumation; ns, no significance; ** $p < 0.01$, *** $p < 0.001$,

dybowskii is associated with energy storage. Most amphibians rely on lipid oxidation to promote metabolism during brumation.¹¹ Interestingly, our findings revealed a contrasting pattern of expression for FFA and TG, with TG levels being lower and FFA levels being higher in the oviduct of *R. dybowskii* in pre-brumation. Similarly, a study on Chinese soft-shelled turtles showed a significant reduction in hepatocyte lipid droplets and hepatic TG content, while the content of FFA was markedly increased during brumation.⁴¹ It is noticed that TG levels exhibited a significant decrease during hibernation compared to the fattening period in female Daurian ground squirrels (*Spermophilus dauricus*).⁴⁰ In this study, our IHC results revealed the expression pattern of TG and FFA synthase and hydrolase enzymes, including Dgat1, Lpl, Hsl, Fasn, Cpt1a, Acadl, and Hadh, in the oviduct during both the

breeding season and pre-brumation. Subsequently, we examined these genes using qRT-PCR. While TG synthesis genes *dgat1* and fatty acid synthesis genes *fasn* displayed no significant differences in mRNA levels between pre-brumation and the breeding season, genes involved in TG hydrolysis to FFA, such as *lpl*, and those associated with FFA oxidation, including *cpt1a*, *acox*, *acadl*, and *hadh*, exhibited a significant increase during pre-brumation. Previous studies have discovered that genes associated with fatty acid metabolism are significantly overexpressed in hibernating Arctic ground squirrels compared to summer-active animals.⁴³ Brumating Chinese soft-shelled turtles have increased mRNA expression levels of lipolysis-related genes and decreased levels of lipogenesis-related genes relative to non-brumating turtles.⁴¹ Therefore, the current results suggest a significant level of TG is

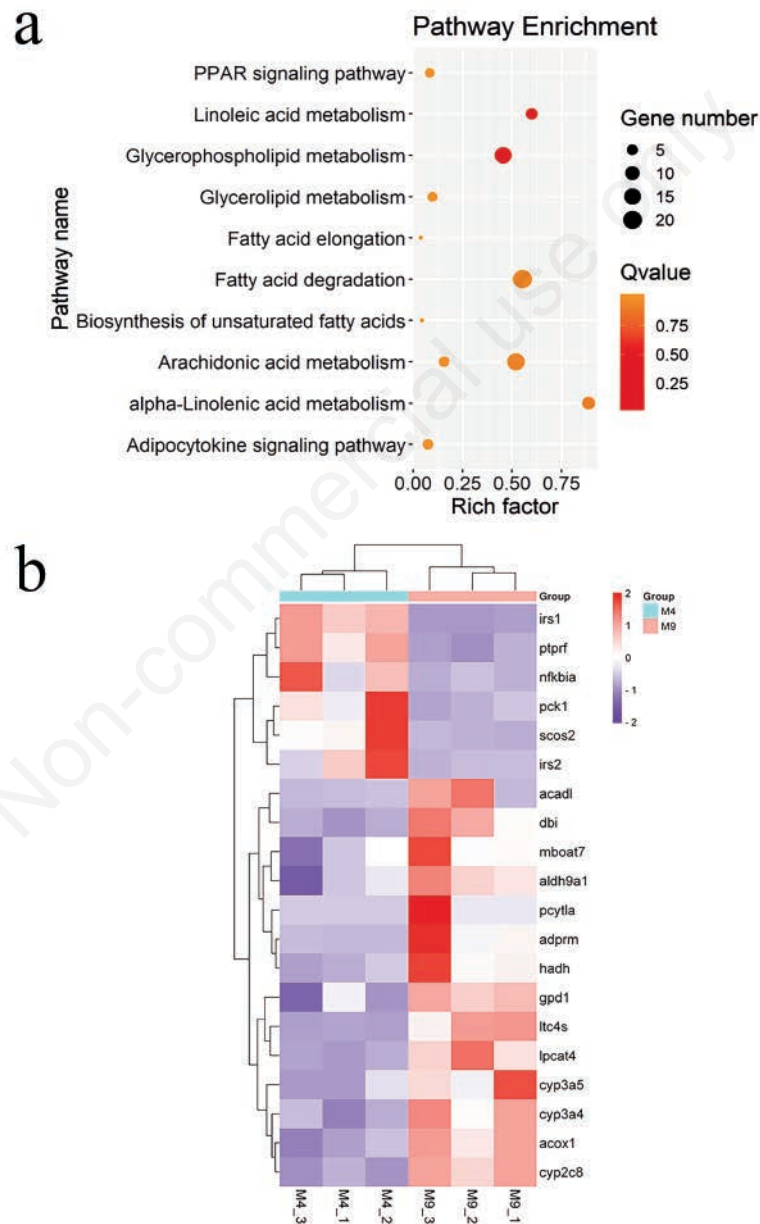


Figure 5. Transcriptomic analysis of lipid metabolism in the oviduct of *R. dybowskii*. KEGG pathway of DEGs linked to lipid metabolism, orange as the bubble color represents insignificant differences and red represents significant differences (a). The heat map of DEGs in lipids metabolism-related pathways. Red color represents highly expressed and blue color represents lowly expressed (b). DEGs, differentially expressed genes. B, breeding season; P, pre-brumation; M4, April; M9, September.

catabolized into FFA during brumation, likely providing energy to *R. dybowskii* through FFA oxidization in the oviduct.

PPAR binds to lipids as a transcriptional activator and regulates genes participated in fatty acid transport and β -oxidation, which are crucial to hibernating survival.⁴⁴ Transcriptomic data from the oviduct of *R. dybowskii* supports the altered lipid metabolism. The PPAR signaling pathway, known for its role in regulating lipid metabolic, was highly enriched in adipose and liver tissues of female alligators during winter suppression.⁷ In our previous studies on *R. dybowskii*, we observed significantly higher levels of PPAR γ -2 protein during pre-brumation in comparison to the breeding season.³⁴ Similarly, protein levels of PPAR γ -2 increased in the liver of food-deficient cavefish compared to sur-

face fish.⁴⁵ Transcriptomic analysis of the *R. dybowskii* oviduct showed the highest content of DEGs in the fatty acid degradation pathway. Therefore, our study further supports the notion that fatty acid oxidation is more significant during pre-brumation.

In this study, transcriptomic and metabolomic data analysis identified several important pathways of lipid metabolism, including linoleic acid metabolism, fatty acid biosynthesis, and α -linolenic acid metabolism. Linoleic acid, a vital fatty acid essential for the functioning of organisms, has the potential to influence the hibernation pattern and the energy expenditure of hibernating animals.⁴⁶ Its deficiency may result in a decreased duration of hibernation periods, heightened energy use, and perhaps reduced survival rates while in hibernation.⁴⁶ Studies in *Nanorana parkeri*

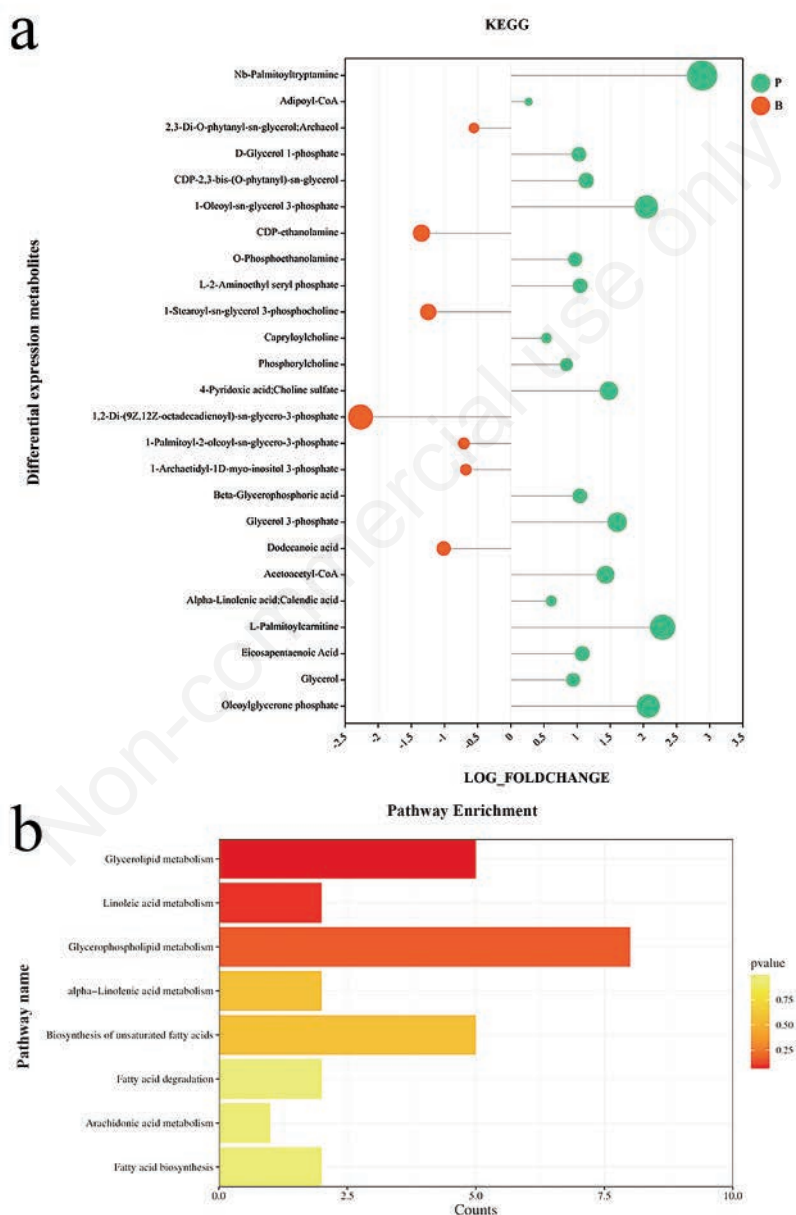


Figure 6. Metabolomic analysis of lipid metabolism in the oviduct of *R. dybowskii*. Lollipop chart map of differential expression metabolites in lipid metabolism pathways. The orange color represents high level of metabolites during the breeding season and the blue color represents high level of metabolites during pre-brumation (a); B, breeding season; P, pre-brumation. KEGG column chart of differential expression metabolites with differential levels in various pathways related to lipid metabolism; Yellow represents insignificant differences and red represents significant differences in the column chart color (b).

have shown that freezing exposure significantly increases the concentration of unsaturated fatty acids in the liver and muscular tissues.⁴⁶ Both the liver's linoleic acid metabolism and the muscle's α -linolenic acid process were drastically altered by the freezing temperature.⁴⁶ A recent study suggested that α -linolenic acid could potentially have an involvement in the process of thermogenesis seen in Arctic ground squirrels during the hibernation period.⁴⁷ Pre-hibernating variable-temperature mammals and species exposed to cold contain more polyunsaturated fatty acids in their body lipids.⁴⁸ The results also clearly demonstrate that polyunsaturated fatty acids, particularly linoleic acid, accumulate in the oviduct before

brumation. This accumulation may play an essential role in the effective overwintering of *R. dybowskii*.

Besides, glycogen and lipids are the major energy stores of frogs.⁴⁹ During the brumation period, there is a reduction or depletion of fat bodies and a decrease in glycogen stores.⁴⁹ Our previous study showed that glycogen synthase catalyzes the formation of more glycogen from glucose, and its protein and mRNA levels were significantly upregulated before brumation.² *R. dybowskii* accumulates large amounts of glycogen before brumation.² Our work reveals that pre-brumation upregulated fatty acid degradation genes compared to breeding season, implying faster metabolism

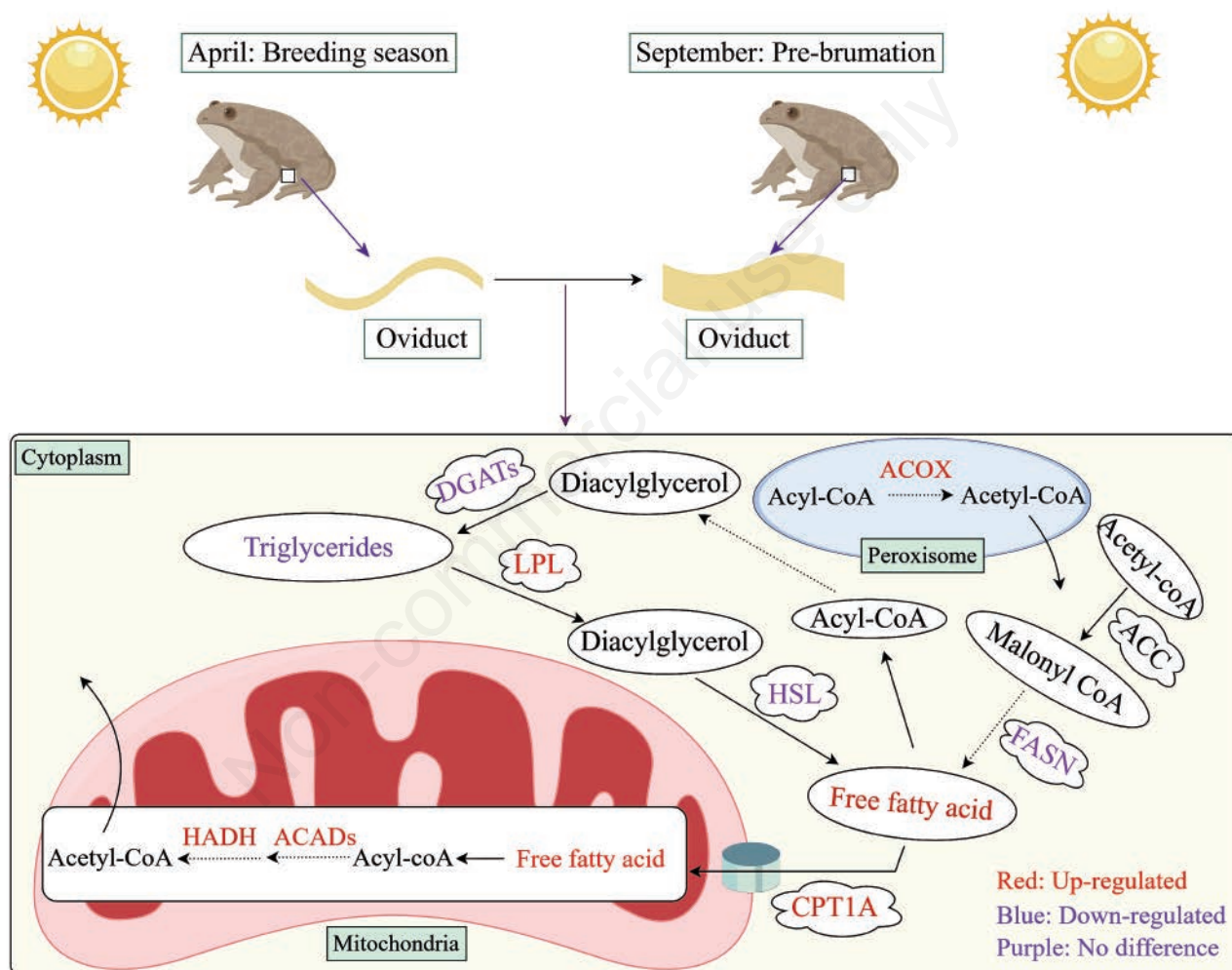


Figure 7. Lipid metabolism in oviductal tissue of *R. dybowskii*. Summary graph of research findings. Triglycerides are typically stored in lipid droplets and can be hydrolyzed into fatty acids by a series of hydrolytic enzymes, such as LPL and HSL. Fatty acids are initially activated to form Acyl-CoA and subsequently converted to triglycerides by DGATs. Acetyl-CoA can generate Malonyl-CoA through ACC, and these two compounds produce fatty acids through the catalytic action of enzymes such as FASN. Fatty acid oxidation typically takes place in the mitochondria, where fatty acids enter through the transport facilitated by CPT1A. Within the mitochondria, enzymatic reactions, including those catalyzed by ACADs and HADH, convert fatty acids to Acetyl-CoA. Additionally, a portion of fatty acid oxidation occurs in peroxisomes, facilitated by ACOXs. Red labeling represented upregulation in pre-brumation oviductal tissue, blue indicated downregulation, and purple represented no significant difference between the breeding season and pre-brumation. Black indicated that no testing was performed. Dashed arrows represented a multi-step reaction, while solid arrows represented a one-step reaction. DGATs, Diacylglycerol acyltransferases; LPL, lipoprotein lipase; ACOX, acyl-CoA oxidase; ACC, acetyl-CoA carboxylase; FASN, fatty acid synthase; HSL, hormone-sensitive lipase; CPT1A, carnitine palmitoyltransferase 1A; HADH, short-chain L-3-hydroxy acyl-CoA dehydrogenase; ACADs, acyl-coenzyme A dehydrogenases. Illustrated by Figdraw.

and oxidation. When fat body is broken down during metabolism, gluconeogenic intermediates are created, including the glycerol moiety of TG, assisting in the development of liver glycogen reserves.¹¹ Glycerol derived from TG breakdown can also serve as a cryoprotectant for gray treefrogs (*Dryophytes chrysoscelis*).⁵⁰ Moreover, the metabolic process of ketones produced by the oxidation of fatty acids decreases the need for available glucose, thus indirectly promoting glycogenesis before hibernation.¹¹ In conclusion, our study suggests that the lipids and glycogen in the oviduct of *R. dybowskii* may work together to provide energy during brumation.

In summary, the investigation of lipid metabolism during brumation in amphibians, with a particular focus on frogs, remains a relatively underexplored research area. This study contributes novel insights by providing the initial comprehensive analysis of lipid synthesis and metabolism in the oviduct of *R. dybowskii*. It reveals that the pre-brumation period is characterized by an accelerated oxidative degradation of TG and a substantial increase in fatty acid levels compared to the breeding season. These findings not only enhance our understanding of amphibian brumation but also pave the way for further investigations into the intricate role of lipid metabolism in this phenomenon.

References

- Niu Y, Cao W, Storey KB, He J, Wang J, Zhang T, et al. Metabolic characteristics of overwintering by the high-altitude dwelling Xizang plateau frog, *Nanorana parkeri*. *J Comp Physiol B* 2020;190:433-44.
- Fan C, Liu Y, Wang Y, Zhang A, Xie W, Zhang H, et al. Expression of glycogenic genes in the oviduct of Chinese brown frog (*Rana dybowskii*) during pre-brumation. *Theriogenology* 2022;185:78-87.
- Wang H, Zhou N, Zhang R, Wu Y, Zhang R, Zhang S. Identification and localization of gastrointestinal hormones in the skin of the bullfrog *Rana catesbeiana* during periods of activity and hibernation. *Acta Histochem* 2014;116:1418-26.
- Green SR, Storey KB. Functional and post-translational characterization of pyruvate dehydrogenase demonstrates repression of activity in the liver but not skeletal muscle of the Richardson's ground squirrel (*Urocyon richardsonii*) during hibernation. *J Therm Biol* 2021;99:102996.
- Scott DE, Casey ED, Donovan MF, Lynch TK. Amphibian lipid levels at metamorphosis correlate to post-metamorphic terrestrial survival. *Oecologia* 2007;153:521-32.
- Otis JP, Sahoo D, Drover VA, Yen CL, Carey HV. Cholesterol and lipoprotein dynamics in a hibernating mammal. *PLoS One* 2011;6:e29111.
- Lin JQ, Huang YY, Bian MY, Wan QH, Fang SG. A unique energy-saving strategy during hibernation revealed by multi-omics analysis in the Chinese alligator. *iScience* 2020;23:101202.
- Rosner E, Voigt CC. Oxidation of linoleic and palmitic acid in pre-hibernating and hibernating common noctule bats revealed by ¹³C breath testing. *J Exp Biol* 2018;221:jeb168096.
- Ensminger DC, Salvador-Pascual A, Arango BG, Allen KN, Vázquez-Medina JP. Fasting ameliorates oxidative stress: A review of physiological strategies across life history events in wild vertebrates. *Comp Biochem Physiol A Mol Integr Physiol* 2021;256:110929.
- Wang G, Kim WK, Cline MA, Gilbert ER. Factors affecting adipose tissue development in chickens: A review. *Poult Sci* 2017;96:3687-99.
- Costanzo JP. Overwintering adaptations and extreme freeze tolerance in a subarctic population of the wood frog, *Rana sylvatica*. *J Comp Physiol B* 2019;189:1-15.
- Maurya RK, Bharti S, Krishnan MY. Triacylglycerols: Fuelling the Hibernating *Mycobacterium tuberculosis*. *Front Cell Infect Microbiol* 2019;8:450.
- Nielsen TS, Jessen N, Jørgensen JO, Møller N, Lund S. Dissecting adipose tissue lipolysis: molecular regulation and implications for metabolic disease. *J Mol Endocrinol* 2014;52:R199-222.
- Tan QQ, Liu W, Zhu F, Lei CL, Wang XP. Fatty acid synthase 2 contributes to diapause preparation in a beetle by regulating lipid accumulation and stress tolerance genes expression. *Sci Rep* 2017;7:40509.
- Chitruju C, Mejhert N, Haas JT, Diaz-Ramirez LG, Grueter CA, Imbriglio JE, et al. Triglyceride synthesis by DGAT1 protects adipocytes from lipid-induced ER stress during lipolysis. *Cell Metab* 2017;26:407-18.e3.
- Lin H, Liu Z, Yang H, Lu L, Chen R, Zhang X, et al. Per- and polyfluoroalkyl substances (PFASs) impair lipid metabolism in *Rana nigromaculata*: A field investigation and laboratory study. *Environ Sci Technol* 2022;56:13222-32.
- Frühbeck G, Méndez-Giménez L, Fernández-Formoso JA, Fernández S, Rodríguez A. Regulation of adipocyte lipolysis. *Nutr Res Rev* 2014;27:63-93.
- Prieto D, Opezzo P. Lipoprotein lipase expression in chronic lymphocytic leukemia: New insights into leukemic progression. *Molecules* 2017;22:2083.
- Steensels S, Ersoy BA. Fatty acid activation in thermogenic adipose tissue. *Biochim Biophys Acta Mol Cell Biol Lipids* 2019;1864:79-90.
- Li Z, Zhang H. Reprogramming of glucose, fatty acid and amino acid metabolism for cancer progression. *Cell Mol Life Sci* 2016;73:377-92.
- Simcox J, Geoghegan G, Maschek JA, Bensard CL, Pasquali M, Miao R, et al. Global analysis of plasma lipids identifies liver-derived acylcarnitines as a fuel source for brown fat thermogenesis. *Cell Metab* 2017;26:509-22.e6.
- Schlaepfer IR, Joshi M. CPT1A-mediated fat oxidation, mechanisms, and therapeutic potential. *Endocrinology* 2020;161:bqz046.
- Li A, Li Y, Wang Y, Wang Y, Li X, Qubi W, et al. ACADL promotes the differentiation of goat intramuscular adipocytes. *Animals* 2023;13:281.
- Joo HJ, Kim KY, Yim YH, Jin YX, Kim H, Kim MY, Paik YK. Contribution of the peroxisomal acox gene to the dynamic balance of daumone production in *Caenorhabditis elegans*. *J Biol Chem* 2010;285:29319-25.
- Shen YQ, Lang BF, Burger G. Diversity and dispersal of a ubiquitous protein family: acyl-CoA dehydrogenases. *Nucleic Acids Res* 2009;37:5619-31.
- Li M, Wang Y, Tang Z, Wang H, Hu J, Bao Z, Hu X. Expression plasticity of peroxisomal acyl-coenzyme A oxidase genes implies their involvement in redox regulation in scallops exposed to PST-producing *Alexandrium*. *Mar Drugs* 2022;20:472.
- Fang H, Li H, Zhang H, Wang S, Xu S, Chang L, et al. Short-chain L-3-hydroxyacyl-CoA dehydrogenase: A novel vital oncogene or tumor suppressor gene in cancers. *Front Pharmacol* 2022;13:1019312.
- Olsen L, Thum E, Rohner N. Lipid metabolism in adaptation to extreme nutritional challenges. *Dev Cell* 2021;56:1417-29.
- Shen Y, Liu Y, Ma J, Ma X, Tian Y, Zhang H, et al. Immunoreactivity of c-kit receptor protein during the pre-hibernation period in the oviduct of the Chinese brown frog, *Rana chensinensis*. *J Vet Med Sci* 2012;74:209-13.
- Xi L, Wang C, Chen P, Yang Q, Hu R, Zhang H, et al.

- Expressions of IL-6, TNF- α and NF- κ B in the skin of Chinese brown frog (*Rana dybowskii*). *Eur J Histochem* 2017;61:2834.
31. Hu R, Xi L, Cao Q, Yang R, Liu Y, Sheng X, et al. The expression of prostaglandin-E2 and its receptor in the oviduct of Chinese brown frog (*Rana dybowskii*). *Prostaglandins Other Lipid Mediat* 2016;124:9-15.
 32. Tang Z, Chen Y, Ren B, Wang X, Zhang H, Han Y, et al. Immunoreactivities of AR, ER α , ER β and aromatase in the nuptial pad of Chinese brown frog (*Rana dybowskii*) during pre-hibernation and the breeding period. *Eur J Histochem* 2021;65:3206.
 33. Zhang Y, Zhang A, Zhao Y, Feng X, Sheng Y, Zhang H, et al. Expressions of TLR4, MyD88, IRAK4 and NF- κ B in the oviduct of Chinese brown frog (*Rana dybowskii*). *Eur J Histochem* 2019;63:3050.
 34. Liu Y, Weng J, Huang S, Shen Y, Sheng X, Han Y, et al. Immunoreactivities of PPAR γ 2, leptin and leptin receptor in oviduct of Chinese brown frog during breeding period and pre-hibernation. *Eur J Histochem* 2014;58:2422.
 35. Guo X, Wang Z, Liu L, Li Y. Transcriptome and metabolome analyses of cold and darkness-induced pellicle cysts of *Scrippsiella trochoidea*. *BMC Genomics* 2021;22:526.
 36. Wang W, Pang J, Zhang F, Sun L, Yang L, Zhao Y, et al. Integrated transcriptomics and metabolomics analysis to characterize alkali stress responses in canola (*Brassica napus* L.). *Plant Physiol Biochem* 2021;166:605-20.
 37. Zhang J, Jiang C, Liu X, Jiang CX, Cao Q, Yu B, et al. The metabolomic profiling identifies N, N-dimethylglycine as a facilitator of dorsal root ganglia neuron axon regeneration after injury. *FASEB J* 2022;36:e22305.
 38. Lin DM, Chen XJ, Wei, YR, Chen Y. The energy accumulation of somatic tissue and reproductive organs in post-recruit female *Illex argentinus* and the relationship with sea surface oceanography. *Fish Res* 2017;185:102-14.
 39. Abdul-Rahman II, Obese FY, Robinson JE, Awumbila B, Jeffcoate IA. Effects of season on the reproductive organs and steroid hormone profiles in guinea hens (*Numida meleagris*). *Br Poult Sci* 2016;57:280-6.
 40. Hurley LL, Crino OL, Rowe M, Griffith SC. Variation in female reproductive tract morphology across the reproductive cycle in the zebra finch. *PeerJ* 2020;8:e10195.
 41. Huang Y, Chen H, Yang P, Bai X, Shi Y, Vistro WA, et al. Hepatic lipid droplet breakdown through lipolysis during hibernation in Chinese Soft-Shell Turtle (*Pelodiscus sinensis*). *Aging (Albany NY)* 2019;11:1990-2002.
 42. Ren Y, Song S, Liu X, Yang M. Phenotypic changes in the metabolic profile and adiponectin activity during seasonal fattening and hibernation in female Daurian ground squirrels (*Spermophilus dauricus*). *Integr Zool* 2022;17:297-310.
 43. Yan J, Burman A, Nichols C, Alila L, Showe LC, Showe MK, et al. Detection of differential gene expression in brown adipose tissue of hibernating arctic ground squirrels with mouse microarrays. *Physiol Genomics* 2006;25:346-53.
 44. Watts AJ, Logan SM, Küber-Heiss A, Posautz A, Stalder G, Painer J, et al. Regulation of peroxisome proliferator-activated receptor pathway during torpor in the Garden dormouse, *Eliomys quercinus*. *Front Physiol* 2020;11:615025.
 45. Xiong S, Wang W, Kenzior A, Olsen L, Krishnan J, Persons J, et al. Enhanced lipogenesis through PPAR γ helps cavefish adapt to food scarcity. *Curr Biol* 2022;32:2272-80.e6.
 46. Niu Y, Cao W, Wang J, He J, Storey KB, Ding L, et al. Freeze tolerance and the underlying metabolite responses in the Xizang plateau frog, *Nanorana parkeri*. *J Comp Physiol B* 2021;191:173-84.
 47. Rice SA, Mikes M, Bibus D, Berdyshev E, Reisz JA, Gehrke S, Bronova I, et al. Omega 3 fatty acids stimulate thermogenesis during torpor in the Arctic Ground Squirrel. *Sci Rep* 2021;11:1340.
 48. Vuarin P, Henry PY, Guesnet P, Alessandri JM, Aujard F, Perret M, Pifferi F. Shallow hypothermia depends on the level of fatty acid unsaturation in adipose and liver tissues in a tropical heterothermic primate. *J Therm Biol* 2014;43:81-8.
 49. Jackson DC, Ultsch GR. Physiology of hibernation under the ice by turtles and frogs. *J Exp Zool A Ecol Genet Physiol* 2010;313:311-27.
 50. Do Amaral MCF, Frisbie J, Goldstein DL, Krane CM. The cryoprotectant system of Cope's gray treefrog, *Dryophytes chrysocelis*: responses to cold acclimation, freezing, and thawing. *J Comp Physiol B* 2018;188:611-21.

Received: 16 October 2023. Accepted: 9 December 2023.

This work is licensed under a Creative Commons Attribution-NonCommercial 4.0 International License (CC BY-NC 4.0).

©Copyright: the Author(s), 2023

Licensee PAGEPress, Italy

European Journal of Histochemistry 2023; 67:3890

doi:10.4081/ejh.2023.3890

Publisher's note: all claims expressed in this article are solely those of the authors and do not necessarily represent those of their affiliated organizations, or those of the publisher, the editors and the reviewers. Any product that may be evaluated in this article or claim that may be made by its manufacturer is not guaranteed or endorsed by the publisher.